Draft version May 27, 2020
Typeset using LaTeX **manuscript** style in AASTeX62

Modeling the Transport Processes of a Pair of Solar Energetic Particle Events Observed by *Parker Solar Probe* near Perihelion

Lulu Zhao,[1] Ming Zhang,[1] and David Lario[2]

[1]*Department of Aerospace, Physics and Space Sciences, Florida Institute of Technology, Melbourne, FL, USA*

[2]*NASA Goddard Space Flight Center, Heliophysics Science Division, Greenbelt, MD, USA*

Submitted to ApJ

ABSTRACT

We present model calculations of the transport processes of solar energetic particles in the corona and interplanetary medium for two events detected by Parker Solar Probe near its second perihelion on 2019 April 2 and April 4. In the 2019 April 2 event, the <100 keV proton differential intensity measured by the IS⊙IS EPI-Lo instrument increased by more than a factor of 10 above the pre-event intensity, whereas the ∼1 MeV proton differential intensity detected by the EPI-Hi instrument did not show any intensity enhancement. In the 2019 April 4 event, the ∼1 MeV proton intensity showed an increase of more than a factor of 100 above the pre-event intensity, but the <100 keV proton intensity enhancement was rather low and gradual. The observational fact that only the 2019 April 4 event displayed a high-energy intensity enhancement indicates that the associated acceleration process in the second event was more energetic than the first event. However, the gradual and low enhancement of the low-energy proton intensity in the second event is at odds with this scenario. In this paper, we investigate the injection

Corresponding author: Lulu Zhao
lzhao@fit.edu

and transport processes of protons in the corona and interplanetary magnetic fields with numerical model simulations. Our model calculations suggest that the gradual and low rise of the low-energy protons in the April 4 event was probably due to the different diffusion conditions in these two events and the fact that the spacecraft was moving away from the source region during these two events.

Keywords: Sun: corona – Sun: particle emission – Sun: magnetic fields – interplanetary medium

1. INTRODUCTION

On 2019 April 2 and April 4, *Parker Solar Probe* (*PSP*) detected a pair of solar energetic particle (SEP) events near its second perihelion at about ~0.17 AU from the Sun. These two events were small, and neither of them were detected by spacecraft near 1 AU. In the 2019 April 2 event, the <100 keV proton intensity measured by the Low-Energy Energetic Particle Instrument (EPI-Lo) of the Integrated Science Investigation of the Sun (IS⊙IS) experiment onboard *PSP* (McComas et al. 2016) increased by more than a factor of 10 above the pre-event measured intensities, whereas the ~1 MeV proton intensity measured by High-Energy Energetic Particle Instrument (EPI-Hi) of IS⊙IS did not show any noticeable enhancement. By contrast, in the 2019 April 4 event, the ~1 MeV proton intensities detected by EPI-Hi did increase by almost a factor of 100 above the pre-event intensities, while the <100 keV proton intensities from EPI-Lo showed only a low gradual increase delayed with respect to the onset of the higher-energy protons.

Figure 1 shows an overview of this time interval. The first three panels show, from top to bottom, (a) the heliocentric radial distance of *PSP*, R_{PSP}; (b) the radial speed V_r of *PSP*; and (c) the azimuthal angular speed ω of *PSP*. The horizontal blue dashed line in Figure 1 (c) indicates the sidereal rotation angular speed of the sun. The vertical dotted line indicates the perihelion passage when R_{PSP} minimized, V_r became zero and ω maximized. Figure 1 (d) shows the intensity-time profiles as detected by the Time-of-Flight (ToF) system of EPI-Lo at three different energies (top three traces) and by the Low Energy Telescope (LET1) of EPI-Hi at about ~1 MeV (black trace).

In all these traces, 60-point moving averages of minute-cadence data are plotted. Each trace is labeled with the energy assigned by the IS⊙IS team under the assumption that particle intensities are dominated by protons. Figure 1 (e) shows 1-minute averages of the proton solar wind speed as measured by the Solar Probe Cup (SPC) of the Solar Wind Electrons Alphas and Protons (SWEAP) experiment on board *PSP* (Kasper et al. 2016). The red trace is a 60-point moving average applied to the 1-min averages. Figure 1 (f) shows 1-minute averages of the magnetic field magnitude as measured by the magnetometers of the FIELDS suite of instruments (Bale et al. 2016) on board *PSP*. The red trace is a 60-point moving average applied to the 1-min averages. Finally, Figure 1 (g) shows the magnetic field magnitude scaled to 1 AU, assuming a $\sim R^2$ dependence.

The two SEP events shown in Figure 1 were first presented by McComas et al. (2019) (see their Figure 4) and studied in detail by Roelof et al. (2019) and Leske et al. (2020). These authors associated the origin of these two events with a single active region visible from the Ahead spacecraft of the *Solar Terrestrial Relations Observatory* (i.e. *STEREO*-A, hereafter *STA*). The Extreme Ultraviolet Imager (EUVI; Wuelser et al. 2004) of the Sun-Earth Connection Coronal and Heliospheric Investigation (SECCHI; Howard et al. 2008) on board *STA* detected small brightness surges moving southward from this active region (see Figure 10 in Leske et al. 2020) that most likely were at the origin of the two SEP events (Roelof et al. 2019). The two purple arrows in Figure 1 (d) indicate the time when the most prominent surges at the origin of the two events occurred (i.e., 09:05 UT on 2019 April 2 and 03:30 UT on 2019 April 4. Note that these times are the times of the *STA*/SECCHI/EUVI observation, and we have subtracted the light transit time from the sun to 1 AU to plot the arrows in Figure 1 (d)). The active region origin of these EUV surges was later numbered NOAA Active Region (AR) 12738 when it rotated into the view of Earth. With respect to *STA*, AR 12738 was located at N13E55 on April 2 and N13E38 on April 4, whereas *PSP* was $\sim 8°$ and $\sim 35°$ westward of STA on April 2 and April 4, respectively. The same active region was also the source of much larger SEP events observed later by *PSP* on April 20-21 (Wiedenbeck et al. 2020; Schwadron et al. 2020).

Apart from the different spectral signatures of both events (i.e. the event on April 2 observed mostly at low (<200 keV) proton energies whereas the event on April 4 being more prominent at >1 MeV proton energies), the event on April 2 displayed enhanced abundances of heavy ions, whereas heavy ion (above He) counts were almost absent on April 4 (see Roelof et al. 2019, and also Figure 4 in Leske et al. (2020)). The two SEP events were highly anisotropic as observed by *PSP*, with intensities measured in the apertures of the *IS*⊙*IS* telescopes looking sunward much larger than those in the opposite direction throughout the event (Leske et al. 2020). An initial ratio between intensities in the anti-sunward and sunward directions along the instantaneous magnetic field direction of ∼20:1 was reported in the April 2 event by Roelof et al. (2019) and in the April 4 event of ∼30:1 by Leske et al. (2020).

Several factors might have played a role in the different properties of these two SEP events, from different properties of the parent solar eruptions to different transport conditions for the protons to propagate from their sources up to *PSP*. In this paper, we analyze the possibility that the signatures of the time intensity profiles in the April 4 event were due to the injection and transport processes in the proximity of the parent active region as well as the effects that the spacecraft's motion had in shaping the time profiles of the SEP events.

2. MODEL SETUP

In this work, the energetic particle transport processes are calculated using the time-forward coronal and interplanetary transport model developed by Zhang & Zhao (2017). This model solves the stochastic differential equations corresponding to the focused transport equation to follow energetic particles' propagation in the corona and interplanetary magnetic fields. All physical processes, including convection, adiabatic deceleration, magnetic focusing, drifts, parallel, and perpendicular diffusion are included (see Zhang & Zhao (2017) for details of the model). We point out that the particle acceleration processes in the source region are not explicitly modeled here. We only consider the transport processes of the particles in the solar corona and interplanetary space once they are released from the injection source region. The coronal magnetic fields between the solar surface (1 R_s) and the solar wind source surface located at 2.5 R_s are calculated by using the potential field source surface (PFSS) model (Altschuler & Newkirk 1969; Schatten et al. 1969; Schrijver & Derosa 2003) based on synoptic magnetograms obtained by the Global Oscillation Network Group (GONG) of the National Solar Observatory (NSO) (https://gong.nso.edu/data/magmap/archive.html). For the April 2 event, we use the synoptic magnetogram at 09:04 UT on April 2, whereas for the April 4 event we use the synoptic magnetogram at 00:14 UT on April 4. A Parker nominal interplanetary magnetic field (IMF) is then assumed beyond 2.5 R_s, with a matching boundary with PFSS at 2.5 R_s. The solar wind speed is assumed to be zero below the source surface. The radial dependence of the solar wind speed above the source surface is calculated based on the empirical electron density formula of Leblanc et al. (1998) using the conservation of mass flow. The asymptotic solar wind speed at large enough radial distance is set to be 350 km s^{-1} as measured in situ by *PSP*.

Protons at energies 40 keV and 1 MeV are injected uniformly and isotropically on the open field lines at three different heliocentric radial distances of 1.05 R_s, 1.5 R_s, and 2.0 R_s. The effect of the magnetic fluctuations on SEP propagation is treated as particle pitch-angle diffusion using the quasi-linear formulation (Jokipii 1966; Schlickeiser 2002). We set the pitch-angle diffusion coefficient equivalent to a constant radial mean free path of 0.1 AU ($\sim$ 20 R_s) for protons at energy of 250 keV around 1 AU. The radial mean free path below the radial distance of 20 R_s is set to be 1/4 times smaller (Zhang & Zhao 2017). And the radial mean free path of 40 keV and 1 MeV protons is determined by assuming a $v^{1/3}$ dependence as a result of a Kolmogorov turbulence spectrum (Kolmogorov 1941). The perpendicular diffusion is treated as a result of the supergranular motion on the photosphere (Zhang & Zhao 2017; Zhao & Zhang 2018). In Zhang & Zhao (2017) and Zhao & Zhang (2018), the perpendicular diffusion coefficient equivalent to a 10% (κ_p) of the supergranular diffusion rate was found to be sufficient to explain the widely spread SEP events that occurred on 2010 February 7 and 2011 November 3. In this work, we adopt the same rate, i.e., 10% of the supergranular motion for the perpendicular diffusion calculation.

3. 2019 APRIL 2 EVENT

On 2019 April 2, the <100 keV proton intensity detected by EPI-Lo started to increase at ∼10:00 UT and remained elevated for about one day, whereas the ∼1 MeV proton intensity detected by EPI-Hi did not show a visible enhancement above the instrument sensitivity (Figure 1 (d)). At 11:00 UT on 2019 April 2, the *PSP*'s Heliocentric Earth Equatorial (HEEQ) coordinates, radial distance, co-latitude, and longitude, were 0.19 AU, 93°, and 89°, respectively. By assuming nominal Parker spiral IMF lines, we calculate the footpoints on the 2.5 R_s source surface of the field lines connecting with *PSP* and with other spacecraft distributed in the heliosphere. The solar wind speed is assumed to be 350 km s^{-1} for *PSP* and 400 km s^{-1} for other spacecraft. The magnetic field line footpoints of the spacecraft on different solar radius from 1 R_s to 2.5 R_s are then calculated using the PFSS coronal magnetic field model.

The synoptic map we used to calculate the coronal magnetic field is built from GONG magnetograms up to 09:04 UT April 2. The coordinates of the *PSP* IMF line footpoints are summarized in the first row of Table 1. In particular, we show the co-latitude (HEEQ co-Lat) and the longitude (HEEQ Lon + 60°) of the magnetic field line footpoints on the 2.5 R_s source surface in columns 5-6, and on the photosphere in columns 7-8. Since the coordinates of the spherical harmonics used to calculate the coronal magnetic field are HEEQ co-latitude and HEEQ longitude + 60° (https://gong.nso.edu/data/magmap/QR/bqc/), the latitudes and longitudes in Table 1 and in the following figures are HEEQ co-Lat and HEEQ Lon+60°.

The loci and footpoints of different spacecraft using nominal Parker IMF lines and PFSS magnetic field lines at 11:00 UT on 2019 April 2 are plotted in the left panels of Figure 2. Green and red areas represent the anti-sunward and sunward open field regions, respectively. The cross symbols represent the magnetic field line footpoints of the spacecraft on the 2.5 R_s source surface and the solid circles represent the footpoints on spheres at, from top to bottom, 1.05 R_s (a), 1.5 R_s (b), and 2 R_s (c), respectively. The black curve is the separatrix of the opposite magnetic field polarities at 2.5 R_s. The location of the active region on the solar surface is indicated by the magenta diamond. *PSP* is represented by the letter P in orange color. Letters A, and E represent *STA* and the *Advanced Composition Explorer* (*ACE*; located at the L1 Sun-Earth Lagrangian point). The footpoints of magnetic field lines connecting to STA and ACE are shown to indicate how other spacecraft are approximately located with respect to the active region.

Usually, the size of the energetic particle injection sources in SEP events can be estimated from the size of the parent coronal mass ejection (CME) or the associated EUV waves (Zhang & Zhao 2017).

An angular radius of 45° and 80° has been assumed to be the injection size in the 2010 February 7 (Zhang & Zhao 2017) and 2011 November 3 (Zhao & Zhang 2018) SEP events. However, the events observed by *PSP* on April 2 and April 4 were too weak to estimate the injection size from coronagraph observations, since both were associated with small surges observed in the EUV images from *STA*. The dashed circles in Figure 2 represent a region around the parent active region with an angular radius of 60°. An injection region with this relatively small radius would allow *PSP* to detect particles without the need to invoke cross-field diffusion. By examining *STA*/EUVI images, the origin of the event on April 2 was found to be associated with brightenings and south-westerly surges observed moving out from the active region 12738 (Roelof et al. 2019). For some of these surges, accompanying EUV waves can be seen moving outward from the active region mainly in the southwestern direction extending over several tens of degrees, which might indicate a continued extended particle injection. Therefore, in the simulation, the injection size is assumed to have an angular radius of 60° to the west of the active region and an angular radius of 50° to the east of the active region.

Particles are released onto open field lines and propagate within the corona. Open magnetic field lines emanate from the active region and expand in both longitude and latitude, allowing the particles to spread toward *PSP*. The projection of the injection locations on the source surface at 2.5 R_s are plotted as green and red dots in the left panels of Figure 3. Green and red colors represent the anti-sunward and sunward magnetic field polarities. All other symbols are the same as in Figure 2. As shown in panels (a) and (b) of Figure 3, with an injection height of 1.05 R_s and 1.5 R_s, particles are injected directly on the magnetic field lines connected to *PSP*. Therefore, *PSP* is expected to detect enhancement with a prompt onset. However, if protons were injected at a higher radial distance of 2.0 R_s as shown in panel (c), *PSP* is not directly connected to the particle injection region and will not detect any particle enhancement, under the assumption that particles strictly follow the magnetic field lines. When including perpendicular diffusion or random walk of field lines, the particles do not just follow the average magnetic field lines depicted by the PFSS model but they can spread to broader regions (Zhang & Zhao 2017; Zhao & Zhang 2018). Furthermore, magnetic field turbulence can scatter particles back and forth and cause them spending more time inside the complex solar coronal magnetic fields.

A total number of more than 2 million protons with an energy of 40 keV are injected uniformly and simultaneously, and their motion is followed for 100 minutes in the time-forward simulation. The left panels of Figure 4 show the relative intensity of all the escaping protons in the reference frame co-rotating with the sun 64 minutes after the initial injection. Here, we consider escaping protons whose final location is above the source surface where field lines are considered completely open. And the intensity level is plotted in log scale. The panels (a), (b), and (c) correspond to the three injection heights of 1.05 R_s, 1.5 R_s, and 2.0 R_s, specified in Figure 2. The intensity level in the field line connecting to *PSP* is similar in panels (a) and (b) because of the direct and uniform injection of particles onto these field lines. The intensity shown in panel (c) is much lower than in (a) and (b). This is because all the particles reach the magnetic field footpoint of *PSP* by cross-field diffusion, which is a slow process.

Using the longitude-latitude distributions shown in the left panels of Figure 4 as an inner boundary (at 0.05 AU from the sun), we performed a time-backward stochastic calculation of particles' propagation. This simulation allows us to conveniently calculate the SEP intensity time profile at the location of *PSP* (Zhang et al. 2009). The radial and perpendicular mean free paths are set to be the same values as the parameters used in the time-forward coronal transport model, i.e. a constant radial mean free path of 0.1 AU for 250 keV protons scaled with particle speed as $\lambda_r{\sim}v^{1/3}$, and 10% of supergranular diffusion as perpendicular diffusion. The injection time profile is assumed to be (Reid 1964; Qin et al. 2006; Zhao et al. 2016)

$$Q = Q_0\frac{1}{t}\exp(-\frac{\tau_r}{t}-\frac{t}{\tau_d}), \tag{1}$$

where τ_r and τ_d indicate the rise and decay timescales of the injection time profile, respectively. These rise and decay timescales are estimated from the time intensity profiles of the energetic particles shown in Figure 1 and can depend on the energy of the particles. Different values of τ_r and τ_d would affect the rise and decay rate of the intensity profile. Q_0 is the normalization constant.

Figure 5 shows the 40 keV proton intensity-time profiles at *PSP* assuming both τ_r and τ_d equal to 0.2 day. Green, red, and blue colors correspond to the three different injection heights. The anti-sunward (outward with a pitch angle of 0° with respect to the magnetic field) and sunward (inward with a pitch angle of 180° with respect to the magnetic field) intensity profiles are plotted in solid and dashed curves, respectively. The difference between the 1.05 R_s and 1.5 R_s injection is small as expected. The intensity level is lower for the 2 R_s injection (blue traces), which is consistent with the distributions of SEPs shown in the left panels of Figure 4. A relatively large outward-to-inward intensity ratio (with a ratio of more than 100) is seen at the beginning of the event and gradually decreases (to ~ 1.5), which is consistent with the observation by Roelof et al. (2019). Figure 6 plots the calculated time intensity profiles assuming different radial mean free paths. The larger the value of the mean free path, the larger the outward/inward ratio (shown by the dotted curves in Figure 6), owing to the less parallel diffusion processes undergone by the particles throughout their transport. The missing of the 1 MeV protons in the April 2 event could be due to the lack of particle acceleration to this high energy by the associated weak eruption. Another reason for the missing of high-energy particles is that the source region of the high-energy particles is far away from the footpoint of *PSP*. We will examine this possibility in the next section when discussing the transport processes in the April 4 event.

4. 2019 APRIL 4 EVENT

On 2019 April 4, the ∼1 MeV proton intensity at *PSP* showed an enhancement by a factor of more than 100 above the pre-event intensity, indicating a relatively stronger event than on 2019 April 2. However, the enhancement of the lower energies (<100 keV) particle intensities was gradual and low (see Figure 1 and also Figure 4 of McComas et al. (2019)). Leske et al. (2020) analyzed the EUVI 195 Å images from *STA* and suggested that the possible sources of energetic particles were southwest directed surges of plasma injection originated from the same active region as associated with the origin of the 2019 April 2 event.

Similar to the April 2 event, we calculate the magnetic field line footpoints of each spacecraft, and the results are shown in the second row of Table 1 and in the right panels of Figure 2. The longitudinal separation between the active region and the footpoint of the magnetic field line connecting to *PSP* on the solar wind source surface at 2.5 R_s (orange crosses in Figure 2) was ∼81°, which is slightly larger than the ∼75° estimated for the April 2 event. If we assume the same SEP injection region, the distance between the magnetic field line footpoint of *PSP* on the source surface and the edge of the SEP source region is larger in the April 4 event. However, the longitudinal separation between the magnetic field line footpoint of *PSP* on the photosphere and the active region as derived from the PFSS model of the April 4 event is just 39°, which is much smaller than the 54° obtained for the April 2 event. Whereas the *PSP* footpoint at 2.5 Rs was more separated from the SEP injection region in the April 4 event than in the April 2 event, the footpoints on the photosphere were closer for the April 4 than for the April 2 event. An energy-dependence of particles injection height could explain the differences between the two events. Assuming the same injection size as for the first event, because the distance between the magnetic field line footpoint of *PSP* and the particle source region changes dramatically with height, the SEP intensity-profile at *PSP* would be different for the two events, since the resulting SEP intensities depend sensitively on the particle injection heights as well as the details of the coronal magnetic field where particles initiate their propagation. Near-the-Sun particle measurements, such as those provided by *PSP*, are more sensitive to those injection and the initial transport processes than measurements at 1 AU.

Viewed from Earth, the active region corresponding to these two SEP events was on the backside of the sun. Therefore, the magnetogram measurements used by GONG to derive the coronal magnetic field configurations are many days old, and hence the PFSS results we use might contain significant uncertainties. To estimate how much uncertainty could be in our calculated magnetic field line footpoints using the PFSS model, we use two other times, 00:14 UT on 2019 March 22 and 00:14 UT on 2019 April 11. The first date, 2019 March 22, was the last day when the parent active region was still within the ±60° field of view from Earth before April 4. The second date, 2019 April 11, was the first day when the parent active region rotated back to the ±60° Earth's field of view. In Table 1 (rows 3 and 4) we have considered the same spatial location of *PSP* as on 2019 April 4 (columns 1-3) and compute field line footpoints at 2.5 R_s (columns 5-6) and 1 R_s (columns 7-8) using the time-displaced PFSS results. The left (right) panels of Figure 7 show the loci and footpoints of each spacecraft using the March 22 (April 11) magnetogram in the same format as Figure 2.

Figure 7 shows that, in contrast to the results shown in Figure 2, the magnetic field line footpoints of *PSP* on the photosphere lie outside the injection region for all injection heights. In addition, the magnetograms obtained on March 22 (left panels in Figure 7) and April 4 (right panels in Figure 4) yield that the *PSP* footpoints on the source surface lie in the northern hemisphere (i.e. north of the neutral line represented by the black wavy line), while the footpoint is in a region of the opposite magnetic polarity if the magnetogram on April 11 is used (right panel in Figure 7). Comparing with the in-situ measurement of the magnetic fields made by FIELDS/*PSP* (Bale et al. 2016), the polarity of the magnetic field was inward as predicted when using the magnetogram on April 11. Here, we do not conclude that the magnetogram on April 11 is more accurate than those on March 22 or April 4 since the *PSP*'s footpoint location is very close to the neutral sheet in the earlier two magnetograms, especially in that on April 4. Using two PFSS coronal magnetic fields constructed before and after the parent eruption of several SEP events, Zhao & Zhang (2018) examined the impact of the small scale variations of the coronal magnetic fields on the transport of energetic particles. They found that the final spatial distribution of energetic particles show only small variations as long as the effect of perpendicular particle diffusion from the random walk of field lines is faster than 10% of the supergranular diffusion rate, and therefore the arrival of SEPs at a spacecraft is not very much affected by the change of small-scale coronal magnetic fields. In the following calculation, we use the coronal magnetic fields reconstructed from the April 4 magnetogram and evaluate the results with the uncertainties of the magnetic fields in the corona.

Since in the 2019 April 4 event, both the high-energy (>1 MeV) and the low-energy (<100 keV) particles were detected, we examine here both 40 keV and 1 MeV protons. To account for the predominantly southwest surges suggested to be responsible for this event (Leske et al. 2020), the area of particle injection is set to be the same as in the April 2 event, i.e. 60° in angular radius to the west of the active region and 50° to the east of the active region. The parallel and perpendicular diffusion is set to be the same as in the case of the April 2 event.

The latitude-longitude distributions of escaping 40 keV protons are shown in the right panels of Figure 4. Since the properties of the latitude-longitude distributions of 40 keV and 1 MeV are similar, we only show here the distribution of 40 keV protons. From top to bottom, the height of particle injection is set at 1.05 R_s, 1.5 R_s, and 2 R_s. As expected, the intensity at the *PSP* magnetic field line footpoint in panel (c) is much lower than these in panels (a) and (b).

The intensity profiles obtained from the time-backward simulations are calculated and shown in Figure 8. The inner boundary location, the diffusion parameters, τ_r and τ_d are assumed to be the same as in the April 2 event. The top panel is for 40 keV protons and the bottom panel for 1 MeV protons. Similar to Figure 5, green, red, and blue colors represent the three different particle injection heights. The anti-sunward (outward) and sunward (inward) intensity profiles are plotted in solid and dashed curves, respectively. The intensity level of 1 MeV proton is determined by assuming a spectral index of -4.3 using a power law fit to the observations between ∼1 and ∼8 MeV in Leske et al. (2020). The overall shape of the calculated 1 MeV proton intensity-time profile agrees with the observation except that the decay is longer than the observation. The longer decay phase of the 1 MeV profile is probably due to the larger than actual decay timescale τ_d assumed in the injection profile specified in Equation 1 (see discussion below). Despite of the small difference between the observation and calculation for the 1 MeV intensity profile, the calculated intensity profile for 40 keV is completely different from the observation. The overall observed intensity is orders of magnitude lower than the simulation results. Figure 8 shows that the intensity level is lower when the injection height is set at 2 R_s because particles are not directly injected onto the magnetic field line connecting to *PSP*. Therefore, one of the possible reasons for the low intensity level of the low-energy particles in April 4 event is that *PSP* was not magnetically connected to the source region. However, as shown in the top panel of Figure 8, with a perpendicular diffusion equals to 10% of the supergranular motion, the ∼40 keV proton intensity profile detected by *PSP* still rises faster and higher than the observation. Therefore, the perpendicular diffusion rate assumed in the April 4 event is probably too large compared to the distance between the source region and the *PSP*'s magnetic footpoint.

To simulate the effect of a decreased perpendicular diffusion, we performed another set of calculations assuming a smaller perpendicular diffusion rate, i.e., $\kappa_p = 1\%$ of the supergranular motion. The latitude-longitude distributions of 40 keV protons assuming different perpendicular diffusion rates, κ_p, are shown in Figure 9. In the top panel, the perpendicular diffusion rate is 10%, whereas in the bottom panel a lower perpendicular diffusion coefficient of 1% the supergranular diffusion rate is assumed. A smaller spread of particles assuming a 1% perpendicular diffusion rate is obtained as expected. In Figure 9, the particle injection height is set to be 1.5 R_s for both panels. Calculations with other values for the particle injection heights show similar results, so they are not shown here.

Whereas a decrease in the perpendicular diffusion rate might contribute to a smaller spread of low-energy particles and a delay in their release from the corona, it is interesting to investigate the effect produced by the spacecraft's motion relative to the source of particles. Figure 1 (c) shows that the angular speed of the spacecraft increased from April 2 to April 4, and moved much faster than the sidereal solar angular speed of 14.7°/day (indicated by the horizontal blue dashed line), especially on April 4. The supercorotation of *PSP* with respect to the sun started around 09:00 UT on April 2 and reached its maximum by the end of April 4. On April 2, the near corotation of *PSP* with the source region facilitates the arrival of particles at the spacecraft, even when the particle injection was weak and lasted for a short time interval because *PSP* was continuously sampling the same field lines filled with low-energy particles. On April 4, *PSP* was continuously moving away from the source region. The supercorotation motion of the spacecraft makes it more difficult for low-energy particles to diffuse across the IMF to reach the magnetic field line that connects to *PSP* at each time.

In order to examine the effects of the decreased perpendicular diffusion and the motion of spacecraft on particle intensity measured at *PSP*, we plot in Figure 10 the different intensity profiles of the outward propagating 40 keV (top panel) and 1 MeV (bottom panel) protons for the April 4 event. τ_r and τ_d are set to be 0.2 day for both energies. Solid (dashed) curves represent the cases when the supercorotation of the *PSP* is (not) considered. The effects of the supercorotation on the intensity profiles are clearly seen. As time goes by, *PSP* moves further away from the source region due to the supercorotation. Therefore, the calculated intensities with supercorotation are lower compared to those without supercorotation. The injection height is set to be 1.5 R_s for the red curves and 2 R_s for the blue and green curves. The perpendicular diffusion rate for the red and blue curves is assumed to be 10% of the supergranular motion and 1% for the green curves. The effects of the supercorotation are more pronounced when the injection height is higher and the perpendicular diffusion rate is smaller. This is because the longitudinal spread of particles is smaller and the magnetic footpoint of *PSP* on the source surface (2.5 R_s) is closer to the edge of the source region, as shown in Figure 4 and Figure 9. Hence, when the supercorotation is considered, the magnetic footpoint connecting to *PSP* continuously moves into regions with lower intensity. In general, to which extent the particles' intensity is affected by the spacecraft's movement depends on the particles' distribution around the spacecraft's magnetic footpoint in the source region.

In Figure 11, we plot the calculated time intensity profiles of the outward propagating 40 keV and 1 MeV protons for the two events. The 40 keV profiles are plotted in red and the 1 MeV profiles are plotted in blue. The relative motion of *PSP* with respect to the source has been taken into consideration for both events indicated by the solid colored curves. The dashed curves are when *PSP* motion is not considered. The time intensity profiles of the 37 keV and 1.09 MeV protons observed by *PSP* are plotted in black. In the April 2 event, the calculated time intensity profiles are normalized with respect to the observation by setting the calculated peak intensity of the 40 keV protons considering the PSP motion (represented by the solid red curve) to be the same as the peak intensity of the 37 keV protons in the observation (represented by the black curve). In the April 4 event, the number of injected 40 keV protons are assumed to be the same as the April 2 event. The intensity level of 1 MeV proton is calculated by assuming a spectral index of -4.3 (Leske et al. 2020). Both solid and dashed curves correspond to an injection time profile follows Equation 1 with τ_r=τ_d=0.2 day; whereas the dotted blue curves have a τ_d=0.08 day with the consideration of *PSP* motion (only plotted for 1 MeV protons). When we assue τ_d=0.2 day, the simulated 1 MeV proton profiles show a decay longer than that observed. In contrast, if τ_d=0.08 day, the simulated 1 MeV proton profiles (dotted lines) fit the decay for the April 4 event. As references, in this figure, we also plot the calculated time intensity profiles of 1 MeV protons shown as the blue curves for the April

2 event. Similar to the April 4 event, the solid blue curve assumes the injection time profile follows Equation 1 with τ_r=τ_d=0.2 day; whereas the dotted blue lines assume τ_d=0.08 day and consider the *PSP* motion. The solid and dotted blue the dotted curves show only a small increase barely visible above the pre-event intensity level. The parallel diffusion parameters in both the April 2 and the April 4 event are set to be the same as those in Figure 5 and Figure 8.

The injection height in calculating the 40 keV proton intensity in April 2 event and the 1 MeV proton intensity in April 4 event is assumed to be 1.5 R_s. In calculating the 40 keV intensity profile of April 4 event and 1 MeV intensity profile of April 2 event, the injection height is assumed to be 2 R_s. The choices of 1.5 R_s injection height and 2 R_s injection height for different cases is to represent the direct and indirect injection of particles onto the *PSP*'s magnetic footpoints. The perpendicular diffusion is assumed to be 10% of the supergranular motion in calculating the 40 keV proton intensity in the April 2 event and 1% of the supergranular motion elsewhere. Note that as long as particles are injected directly onto the magnetic footpoints of *PSP*, the effect of the perpendicular diffusion rate on the time-intensity profiles is negligible.

Although the *PSP* angular speed is smaller in time period of the April 2 event than that in the April 4 event, the reduction in particle intensity due to the supercorotation effect (i.e. the difference between the solid and dashed lines in Figure 10) seems to be larger in the April 2 event compared to that in the April 4 event. This is because the extent to which the particle intensity is reduced depends not only on the angular speed of the spacecraft moving away form the active region but also on the distribution of particles around the injection particle source region. Although the particles are initially injected on the open field regions uniformly, their spatial distributions are changed by the complex coronal magnetic fields and diffusion processes. In the April 2 event, the intensity gradient around the *PSP*'s magnetic footpoint is larger than that in the April 4 event. Therefore, as *PSP* moves away from the injection source, the field line connecting to *PSP* at each moment is less and less populated with energetic particles in the April 2 event than in the April 4 event. Figure 11 shows that if energetic particles are not injected directly onto the footpoint of *PSP* (i.e. injection height at $\geq$2 R_s), a weaker perpendicular diffusion rate together with the supercorotation of the spacecraft lead to a delayed and slower onset of 40 keV protons, comparable to the observations.

5. DISCUSSION AND CONCLUSION

We have studied a pair of SEP events observed by *PSP* when it passed its second perihelion using a coronal and interplanetary particle transport model. Both events were small in intensity and size and they were not observed by spacecraft at 1 AU. Persistence of magnetic-field-aligned ion streaming anisotropies away from the sun in these two events (McComas et al. 2019) indicates that protons arrived onto the field lines connected to *PSP*. The first event was weak, with only the low-energy protons showing intensity enhancements. The second event was more energetic, with the intensity of >1 MeV protons increasing by more than a factor of 100 above pre-event intensities. However, the enhancement of the <100 keV protons in the second event was relatively weak. If the particles were injected from the same source region in the two events, the distance between the magnetic field line footpoint of *PSP* and the source region changed, not only because of the change of the *PSP* location relative to the parent active region, but also because the variations in the complex coronal magnetic field configuration.

From previous studies, the calculated magnetic field line footpoints strongly depends on the details of the coronal magnetic models. If the magnetic field line of *PSP* is close to the edge of the SEP source region, which is likely to be the case for these two events, a slight variation of the footpoint location would affect the intensity profile observed by *PSP* significantly. In this work, a nominal Parker IMF model with a constant radial solar wind speed of 350 km s^{-1} as obtained from observations is used to trace the magnetic connection from the *PSP*'s location back to the solar wind source surface. From the source surface to the photosphere, we use a coronal magnetic field derived from the PFSS method with the NSO/GONG synoptic maps built from magnetogram measurements to trace the field line to the photosphere. The synoptic maps obtained from NSO/GONG magnetograms are only up-to-date when the measured region is facing Earth within approximately ±60° (Nitta & Derosa 2008; Schrijver & Title 2011; Riley et al. 2006). However, the active region responsible for producing and releasing SEPs in the two events was on the backside of the sun as viewed from Earth. Therefore, the uncertainty of the magnetogram close to the active region could be considerable. We also traced the magnetic footpoints of *PSP* using magnetograms at two very different times, March 22 and April 11, corresponding to the last and first appearances of the active region within the ±60° field of view from Earth before and after the events. The longitudinal distances between the magnetic field line footpoint of *PSP* on the photosphere and the active region were $\sim 71^\circ$ and $\sim 87^\circ$ in these two cases, which are larger than the $\sim 39^\circ$ obtained using the magnetogram on April 4. Furthermore, the coronal magnetic field may vary even if it is reconstructed from the same source of photospheric magnetic field measurements using different field models. Such a situation could be particularly compromised if the field lines go through regions of weak magnetic fields where the field structure is sensitive to the field models and data input.

Despite all these uncertainties, the PFSS model could be a good approximation of the global coronal magnetic field structures for these two events, when the solar activity is low and the impact of the non potential transient events and active regions is small (Bale et al. 2019). If the height and size of the particles' injection is fixed, different configurations of the coronal magnetic fields determine whether energetic particles are released directly onto the magnetic field lines that connect to *PSP*. When the energetic protons are not directly injected onto the connected magnetic field lines, the efficiency of the cross-field diffusion determines the particle enhancement profiles. Moreover, since *PSP* was continuously moving away from the source region during the time period of these two events, the profiles of the low-energy particles will be affected more than the profiles of the high-energy profiles because it takes more time for the low-energy particles to reach the observation site. The gradual and low-intensity of the <100 keV protons in the second event can then be explained by an indirect injection, a decreased perpendicular diffusion strength and the supercorotation of the spacecraft with respect to the parent active region.

The supercorotation of *PSP*, that will repeat near its perihelia throughout the *PSP* mission, represent a challenge to correctly interpret energetic particle data from this spacecraft. During these periods, the magnetic connection between *PSP* and the particle sources continuously changes, following a pattern opposite to what we have been habituated to interpret observations from 1 AU.

Whereas the injection of low-energy particles from a particle source is usually more abundant than that of high-energy particles, the transport conditions of these particles to reach a spacecraft that moves away from the particle source might lead to situations when intensity enhancements are more significant at high than at low energies. The occurrence of more intense events throughout solar cycle 25, with the capability to fill broad extents of the inner heliosphere, will most likely obscure this effect, and hence the importance to analyze and understand these first small SEP events observed by *PSP*.

L. Zhao and M. Zhang are supported in part by NASA under Grants NNX15AB76G, 80NSSC19K0076, 80NSSC18K0644, 80NSSC20K0286, and 80NSSC20K0298. D. Lario was supported by NASA-HGI grant NNX16AF73G and NASA/LWS grant NNX15AD03G, and NASA program NNH17ZDA001N-LWS. We acknowledge the NASA Parker Solar Probe mission team and the SWEAP team led by J. C. Kasper, the IS$\odot$IS team led by D. J. McComas, and the FIELDS team led by S. D. Bale for use of data. Data used in this paper can be downloaded from spdf.gsfc.nasa.gov. Parker Solar Probe was designed, built, and is now operated by the Johns Hopkins Applied Physics Laboratory as part of NASAs Living with a Star (LWS) program (contract NNN06AA01C). Support from the LWS management and technical team has played a critical role in the success of the Parker Solar Probe mission. This work utilizes data obtained by the Global Oscillation Network Group (GONG) program, managed by the National Solar Observatory and operated by AURA, Inc. under a cooperative agreement with the National Science Foundation. The solar photospheric magetogram data are acquired by instruments operated by the Big Bear Solar Observatory, High Altitude Observatory, Learmonth Solar Observatory, Udaipur Solar Observatory, Instituto de Astrofisica de Canarias, and Cerro Tololo Interamerican Observatory.

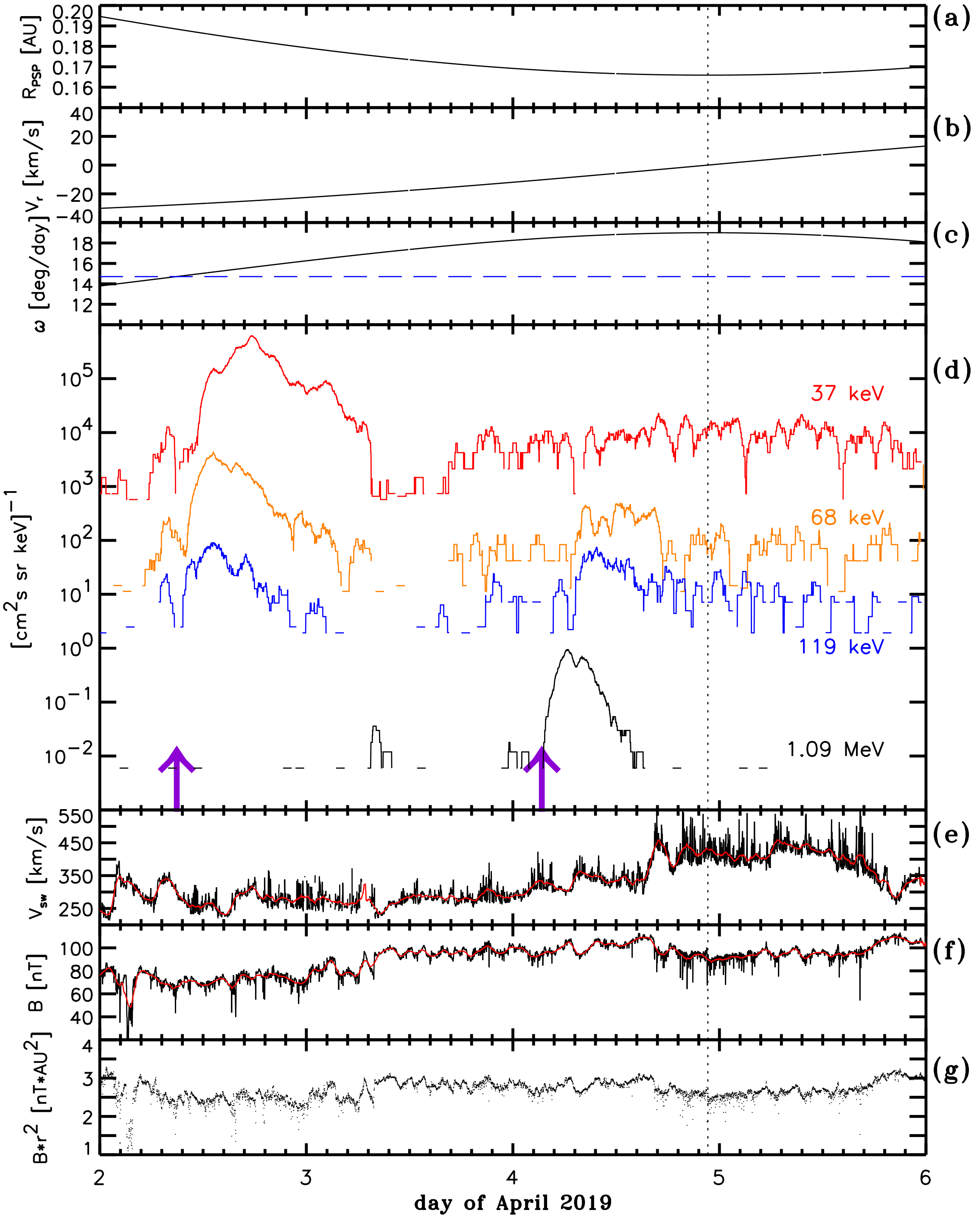

Figure 1. Overview of the *PSP* measurements from 2019 April 2 to 2019 April 6. From top to bottom, (a) *PSP* heliocentric radial distance, (b) *PSP* radial speed, and (c) *PSP* azimuthal angular speed. The dashed blue horizontal line in panel (c) plots the sidereal rotation speed of the Sun. (d) Proton intensity-time profiles at four different energies measured by EPI-Hi and EPI-Lo. (e) Solar wind speed measured by *PSP*/SWEAP. (f) Magnitude of the magnetic field as measured by *PSP*/FIELDS, and (g) magnetic field magnitude scaled to 1 AU, assuming a $\sim R^2$ dependence.

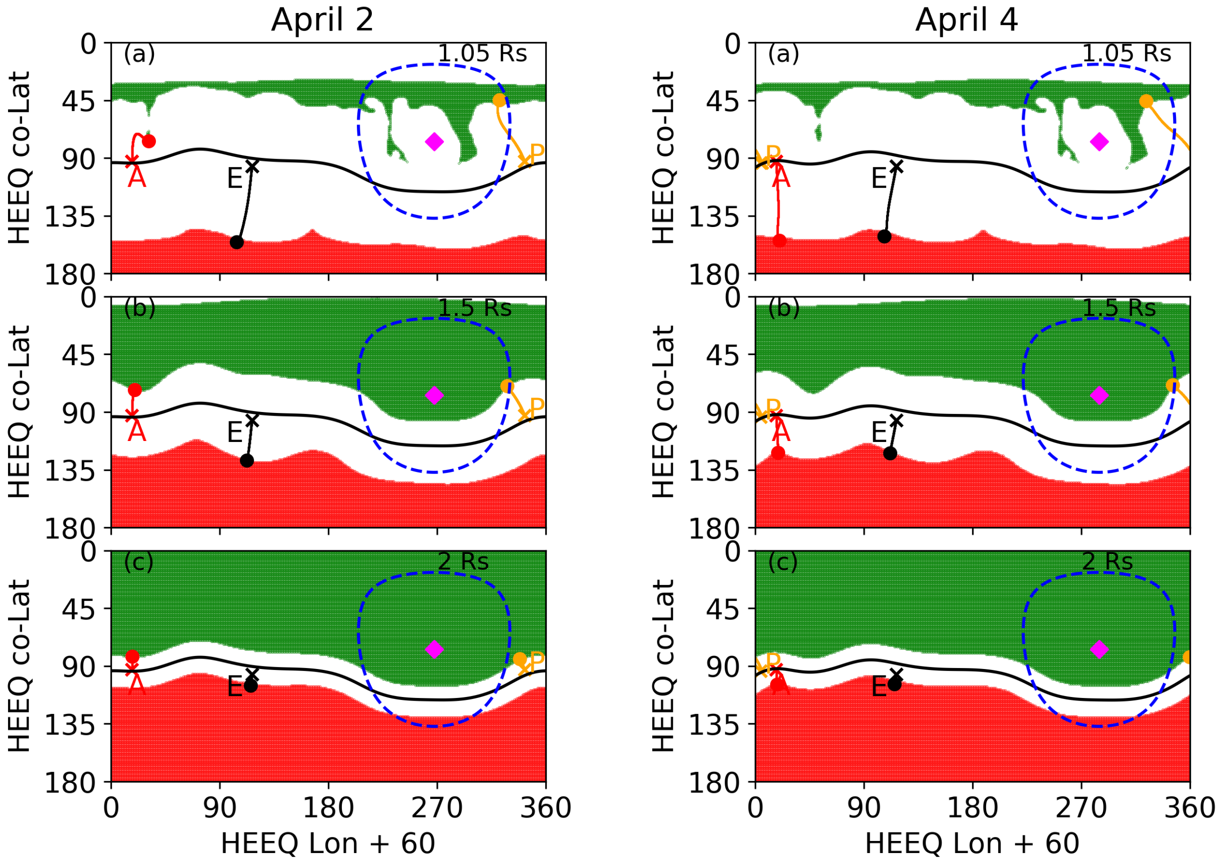

Figure 2. Loci of open fields calculated from the PFSS coronal magnetic field model using the synoptic maps at 09:04 UT 2019 April 2 (left) and 00:14 UT 2019 April 4 (right). The green dots are Anti-sunward and the red dots are sunward open fields on spheres of radius 1.05 R_s (panel (a)) , 1.5 R_s (panel (b)) and 2 R_s (panel (c)). The magenta diamond symbol is the estimated active region location. The black curve is the separatrix between the opposite magnetic field polarities. The magnetic field line footpoints of spacecraft on the 2.5 R_s solar wind source surface are indicated by the cross symbols, and the solid circles are their footpoints on 1.05 R_s (panel (a)), 1.5 R_s (panel (b)), and 2 R_s (panel (c)). The spacecraft *STA* is plotted in red, *ACE* in black, and *PSP* in orange. The dashed circle represents the area of 60° angular radius centered at the active region.

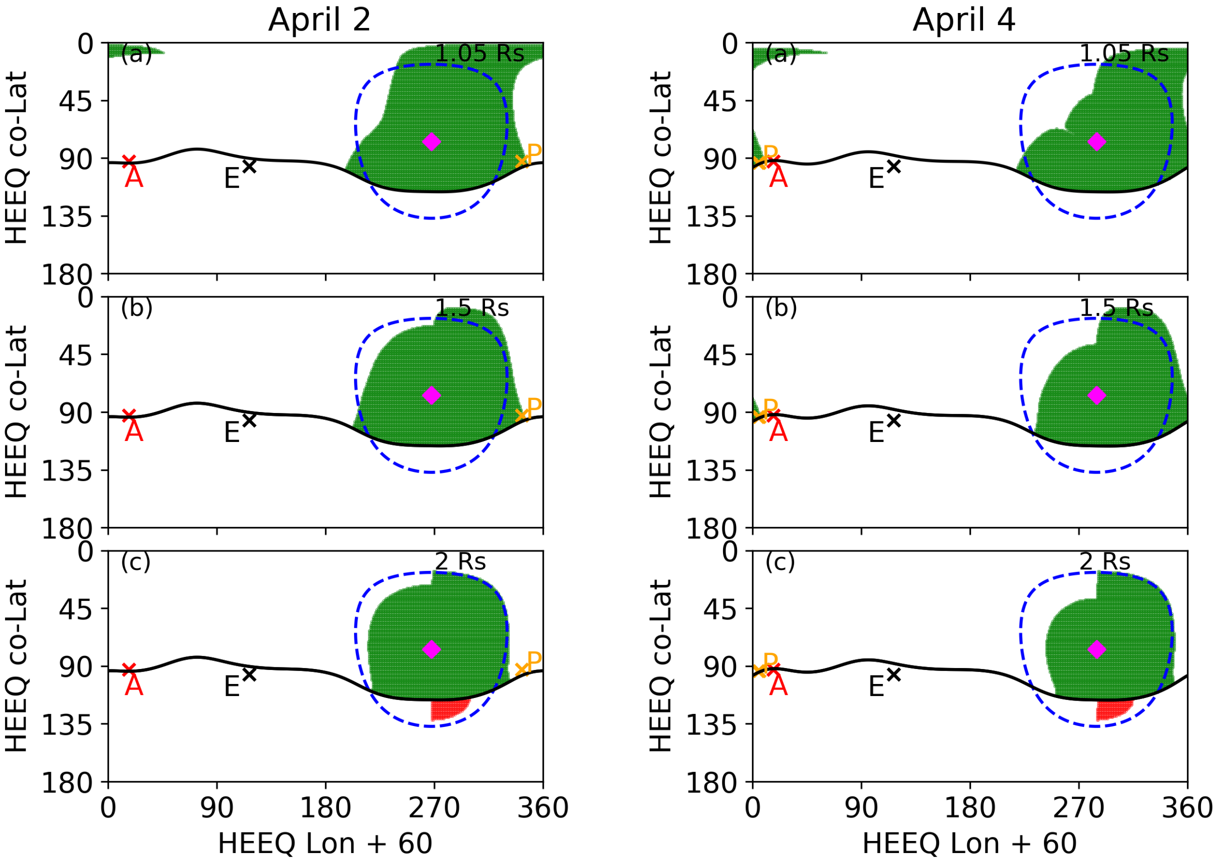

Figure 3. The same as Figure 2 except all the green (anit-sunward) and red (sunward) dots are the projection of all the injection locations onto the solar wind source surface of 2.5 R_s.

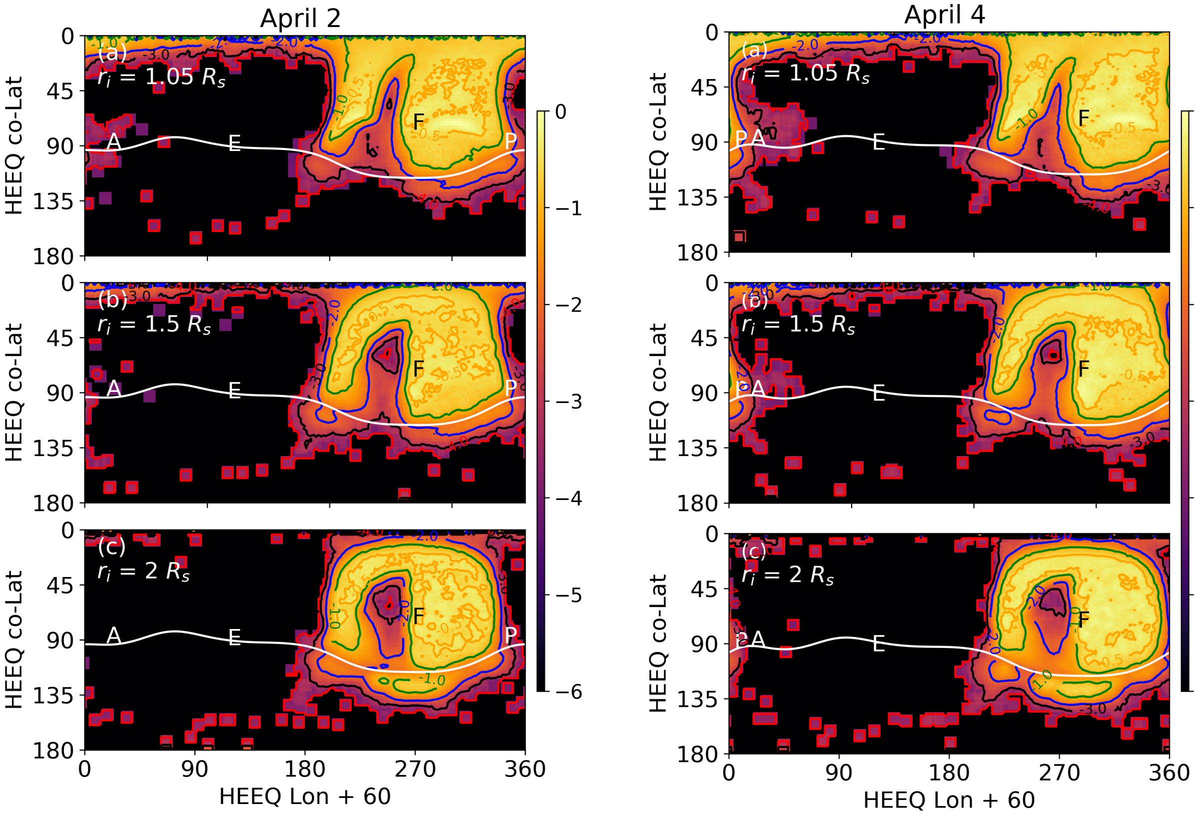

Figure 4. The magnetic field line footpoint distribution of the escaping proton locations on the solar wind source surface (2.5 R_s) at the time 64 minutes after injection for the April 2 event (left) and the April 4 event (right) event. The particle injection height is 1.05 R_s, 1.5 R_s, and 2 R_s, for panel (a), (b), and (c) respectively. The white curve is the separatrix between the opposite magnetic field polarities. Letters A, B, E, and P mark the footpoint location of spacecraft on the source surface.

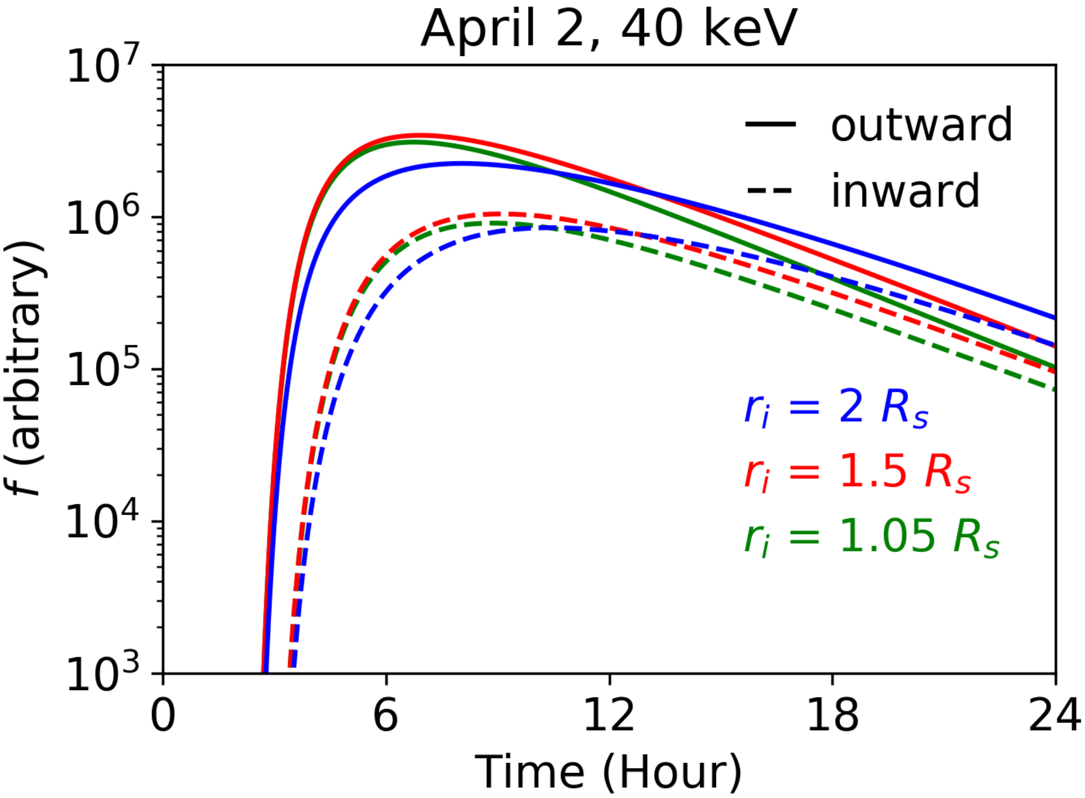

Figure 5. The calculated time intensity profiles of 40 keV protons for the April 2 event. Green, red, blue colors represent different injection heights. The intensity profiles of outward and inward moving particles are plotted in solid and dashed curves respectively.

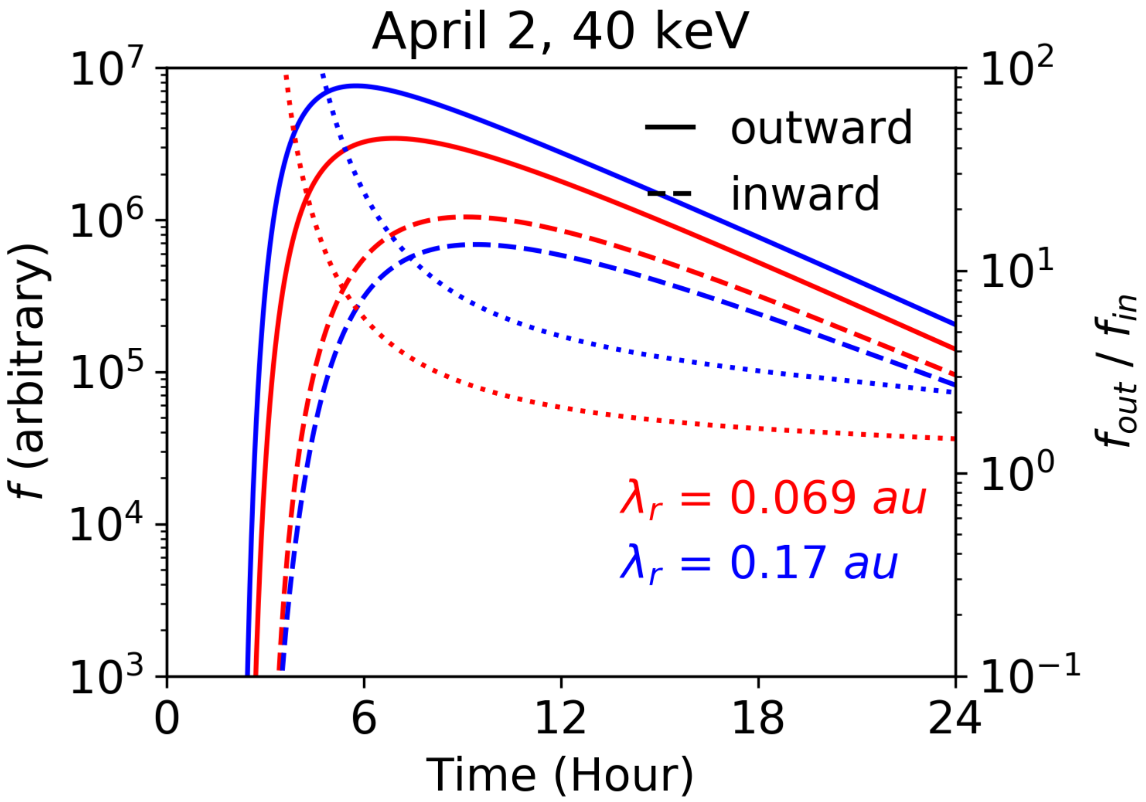

Figure 6. The calculated time intensity profiles of 40 keV protons for the April 2 event. Red, blue colors indicates different radial mean free paths. The intensity profiles of outward and inward moving particles are plotted in solid and dashed curves. The dotted curves plot the ratio of the outward and inward moving particle intensity.

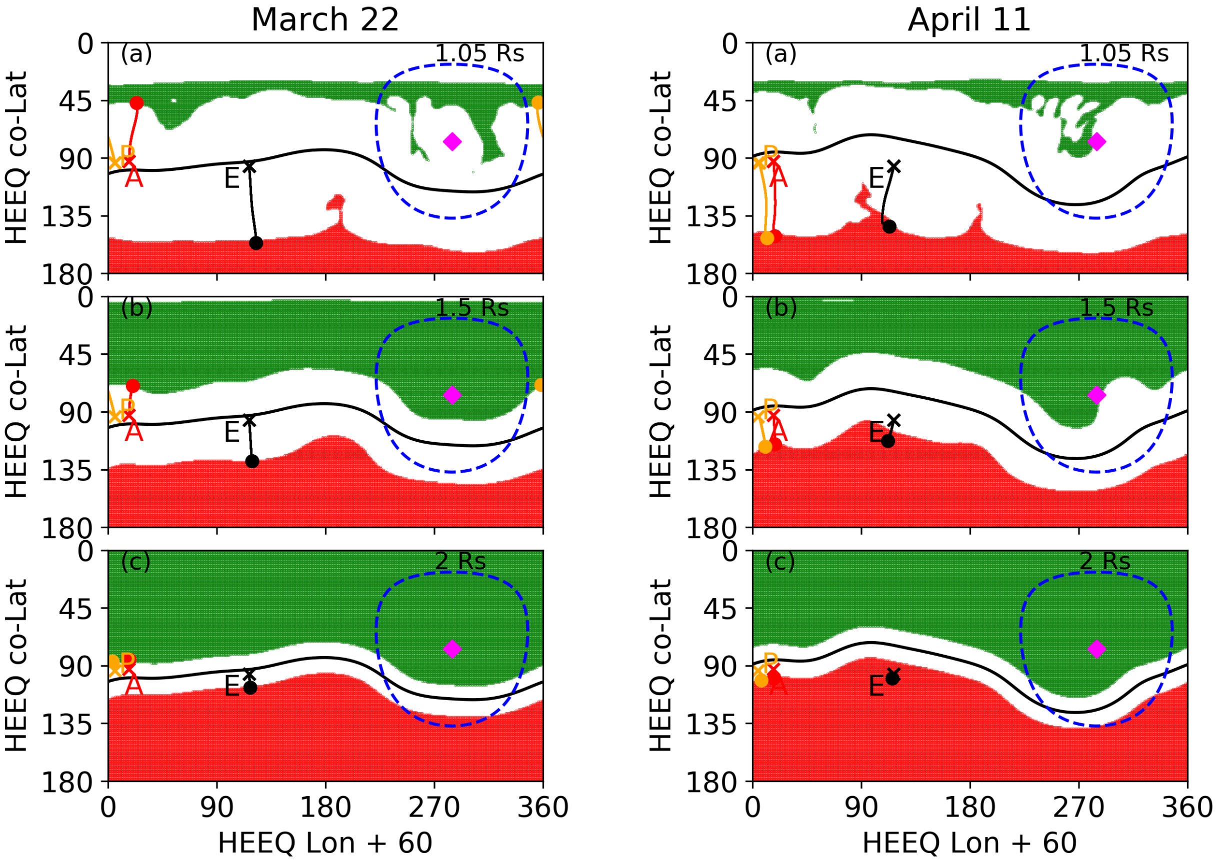

Figure 7. The same as Figure 2 except the coronal magnetic field model are taken from the magnetogram measurements at the time of 00:14 UT 2019 March 22 (left) and 00:14 UT 2019 April 11 (right).

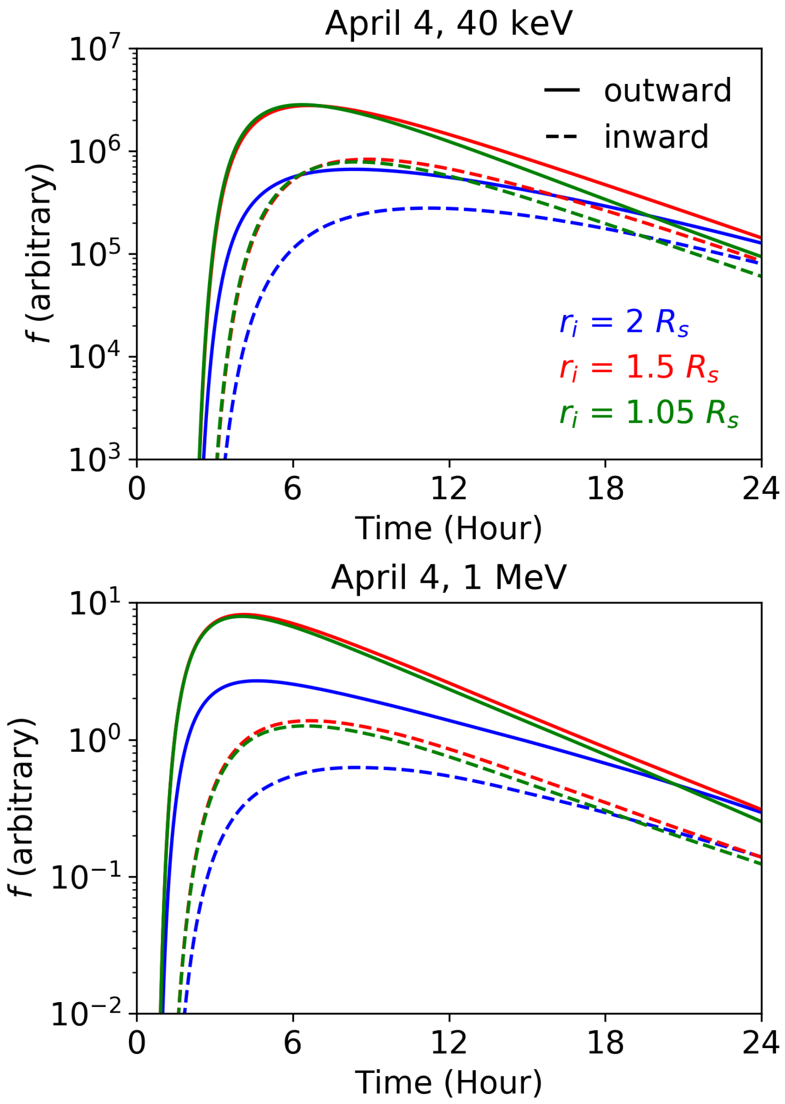

Figure 8. The calculated time intensity profiles of 40 keV (top) and 1 MeV (bottom) protons for the April 4 event. Green, red, blue colors represent different injection heights. The intensity profiles of outward and inward moving particles are plotted in solid and dashed curves.

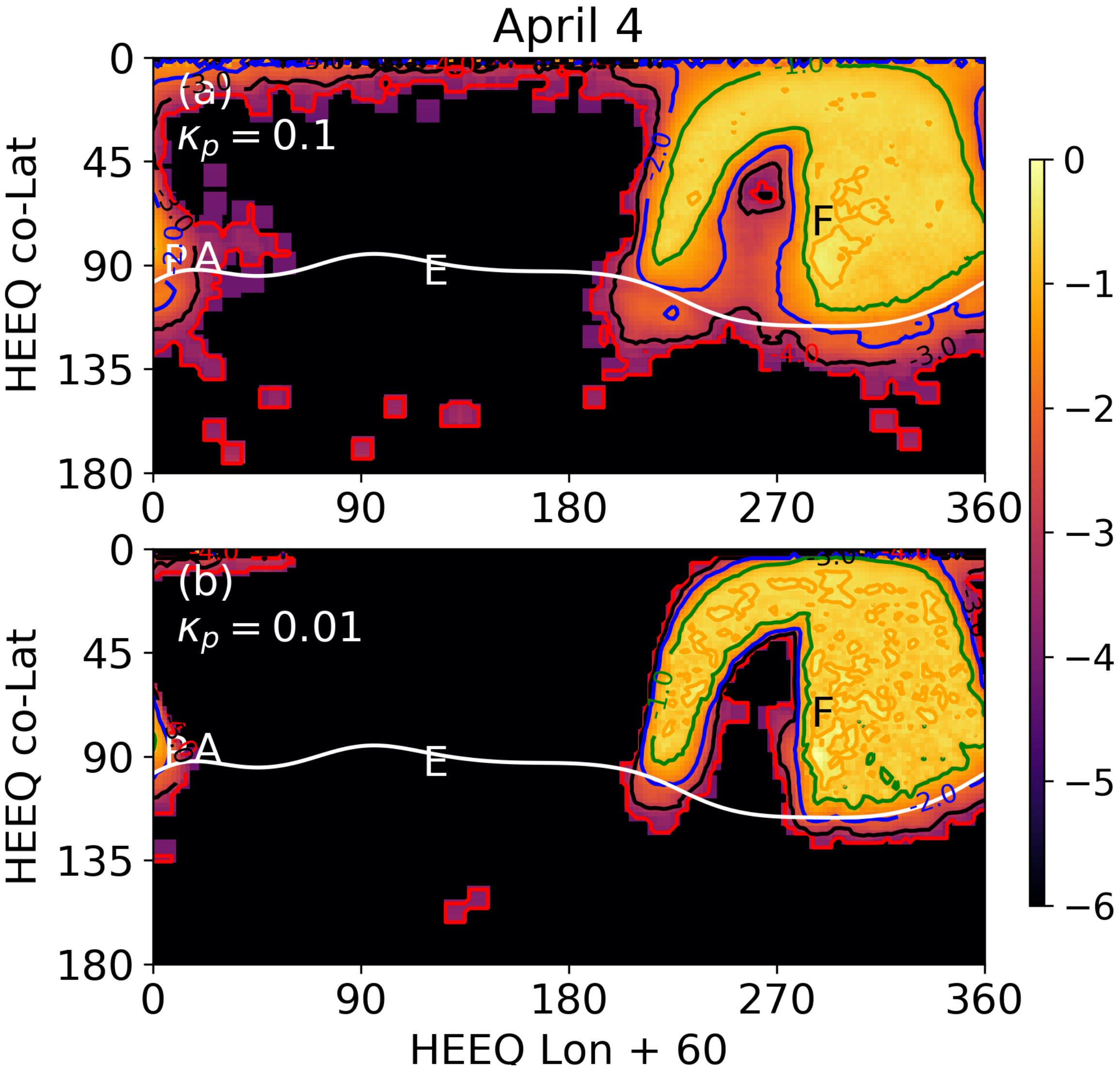

Figure 9. The magnetic field line footpoint distribution of the escaping protons on the solar wind source surface (2.5 R_s) at the time 64 minutes after particle injection for the April 4 event with a diffusion coefficient of 10% (top) and 1% (bottom) the supergranular diffusion rate. The injection height is set to be 1.5 R_s. All other symbols are the same as Figure 4.

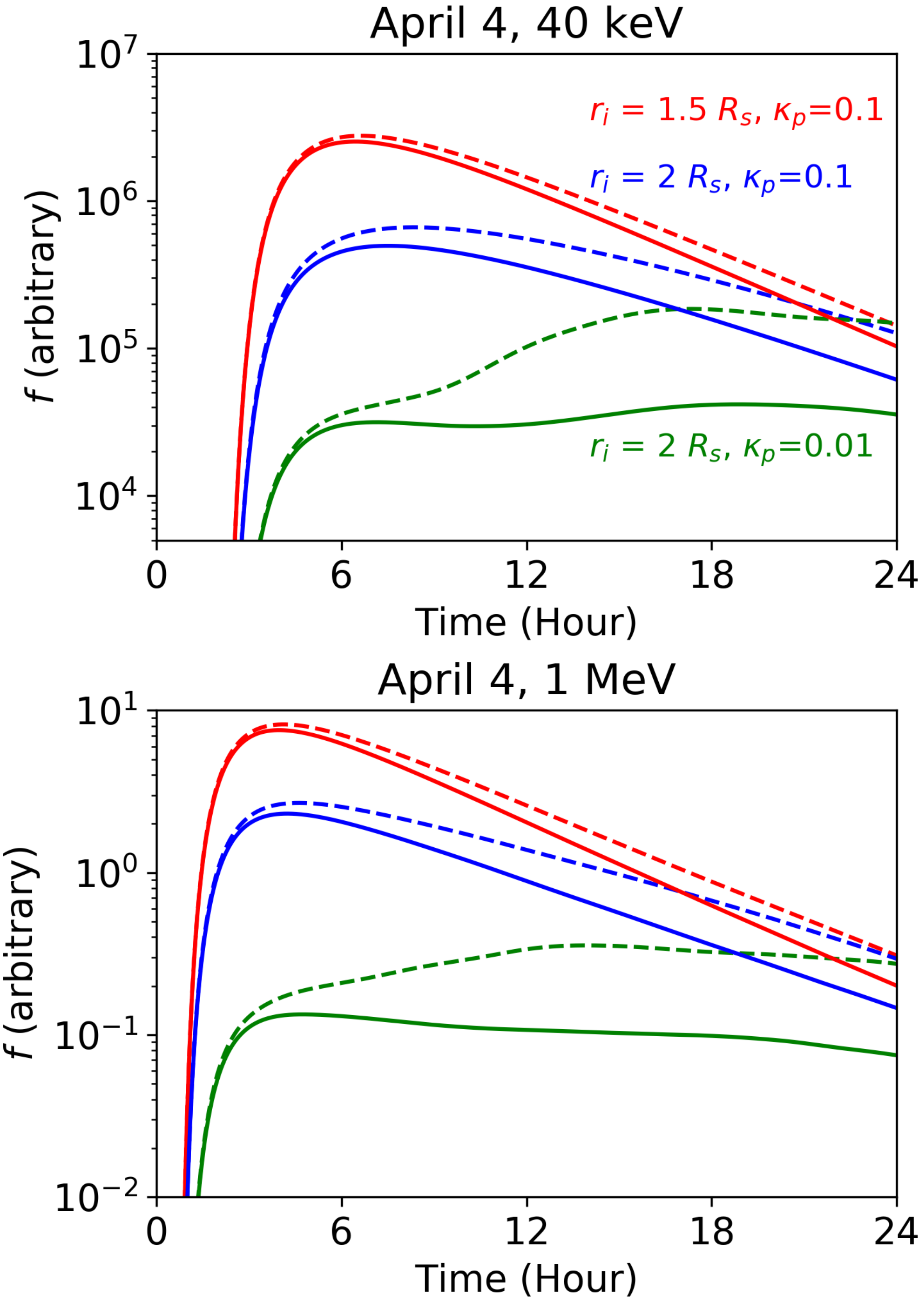

Figure 10. The calculated 40 keV (top) and 1 MeV (bottom) outward proton time-intensity profiles in the April 4 event. The solid (dashed) curves plot the time intensity profiles with (without) considering the supercorotation of *PSP*. The perpendicular diffusion is assumed to be 10% of the supergranular motion for the red and blue curves, and 1% for the green curves.

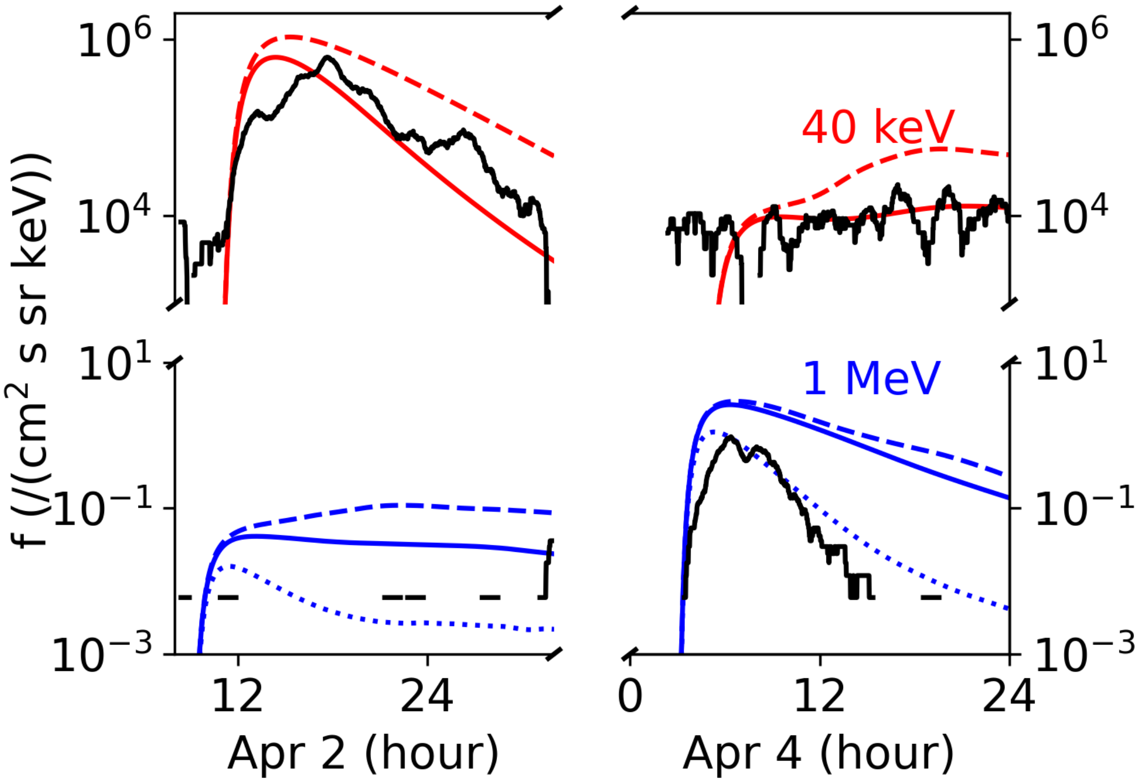

Figure 11. The outward propagating 40 keV and 1 MeV proton time-intensity profiles for the April 2 and the April 4 event. The *PSP* observations are plotted in black and the numerical calculations are plotted in red (40 keV) and blue (1 MeV). The solid and dotted curves plot the intensity profiles considering the supercorotation of *PSP*. The dashed curves do not consider the supercorotation. The solid and dashed curves correspond to the case when the decay time scale (τ_d) of the injection profile is 0.2 day. The dotted curves assume the decay time scale, τ_d, is 0.08 day (only plotted for 1 MeV protons).

Table 1. Magnetic Field Line Footprint of *PSP*

Event	*PSP* location			2.5 R_s		1 R_s	
	r (AU)	co-Lat	Lon+60	co-Lat	Lon+60	co-Lat	Lon+60
April 2	0.19	93	331	93	342	45	322
April 4	0.17	94	355	94	5	45	324
March 22	0.17	94	355	94	5	47	356
April 11	0.17	94	355	94	5	153	12

NOTE—The magnetic field line footpoints of *PSP* in the 2019 April 2 and 4 events. Columns 2-4 show the spacecraft locations. Columns 5-6 show the magnetic field line footpoints on the source surface (2.5 R_s) that connect to the spacecraft. Columns 7-8 show the footpoints on the photosphere (1 R_s) obtained by tracing along the magnetic field line from 2.5 R_s to 1 R_s using the PFSS model. The longitude and latitude are given in the HEEQ coordinates in the unit of degree.

REFERENCES

Altschuler, M. D., & Newkirk, G. 1969, Sol. Phys., 9, 131

Bale, S. D., Goetz, K., Harvey, P. R., et al. 2016, Space Sci. Rev., 204, 49

Bale, S. D., Badman, S. T., Bonnell, J. W., et al. 2019, Nature, 576, 237

Howard, R. A., Moses, J. D., Vourlidas, A., et al. 2008, Space Sci. Rev., 136, 67

Jokipii, J. R. 1966, Astrophys. J., 146, 480

Kasper, J. C., Abiad, R., Austin, G., et al. 2016, Space Sci. Rev., 204, 131

Kolmogorov, A. N. 1941, Dokl. Akad. Nauk. SSSR, 30, 301

Leblanc, Y., Dulk, G., & Bougeret, J. 1998, Sol. Phys., 183, 165

Leske, R. A., Christian, E. R., Cohen, C. M. S., et al. 2020, Astrophys. J., 246, 1

McComas, D. J., Alexander, N., Angold, N., et al. 2016, Space Sci. Rev., 204, 187

McComas, D. J., Christian, E. R., Cohen, C. M., et al. 2019, Nature, 576, doi:10.1038/s41586-019-1811-1

Nitta, N. V., & Derosa, M. L. 2008, Astrophys. J., 673, 207

Qin, G., Zhang, M., & Dwyer, J. R. 2006, J. Geophys. Res., 111, A08101

Reid, G. C. 1964, J. Geophys. Res., 69, 2659

Riley, P., Linker, J. A., & Mikic, Z. 2006, Astrophys. J., 653, 1510

Roelof, E. C., Allen, R. C., Bale, S. D., et al. 2019, American Geophysical Union Abstract

Schatten, K., Wilcox, J., & Ness, N. 1969, Sol. Phys., 9, 131

Schlickeiser, R. 2002, Cosmic Ray Astrophysics (Springer Berlin Heidelberg)

Schrijver, C. J., & Derosa, M. L. 2003, Sol. Phys., 212, 165

Schrijver, C. J., & Title, A. M. 2011, J. Geophys. Res., 116, 1

Schwadron, N. A., Bale, S., Bonnell, J., & et al. 2020, ApJS, 246, 33

Wiedenbeck, M. E., Allen, R. C., Bale, S., & et al. 2020, ApJS, 246, 42

Wuelser, J.-P., Lemen, J. R., Tarbell, T. D., et al. 2004, Telesc. Instrum. Sol. Astrophys., 5171, 111

Zhang, M., Qin, G., & Rassoul, H. 2009, Astrophys. J., 692, 109

Zhang, M., & Zhao, L. 2017, Astrophys. J., 846, 107

Zhao, L., & Zhang, M. 2018, Astrophys. J. Lett., 859, L29

Zhao, L., Zhang, M., & Rassoul, H. K. 2016, Astrophys. J., 821, 62